ELSEVIER

International Journal of Mass Spectrometry 198 (2000) 97–111

International Journal of Mass Spectrometry

Opportunities for optimization of the rf signal applied to electrodes of quadrupole mass spectrometers. Part II. EC signals

Ernst P. Sheretov*, Boris I. Kolotilin, Nikolay V. Veselkin, Alexander V. Brykov, Edgar V. Fedosov

Department of Physics, Ryazan State Radio Technical University, 391000 Ryazan, Russia

Received 12 August 1999; accepted 4 January 2000

Abstract

In this article we discuss the use of harmonic and pulse EC signals in quadrupole mass spectrometers (QMS). Described are the structure of these signals, stability diagrams, and features of the amplitude-phase characteristics. We show that use of such signals can dramatically increase sensitivity of the QMS, and this increase is a direct result of the amplitude-phase characteristic's specific shape. Performance of the ion trap driven by a pulse EC signal and meander are compared. Experiments show that an increase in sensitivity achieved by the EC signal simplifies the implementation of the QMS operating modes in the upper zones of the stability diagram. We provide an example in which the EC signal is used to operate a quadrupole mass filter in the upper zones. (Int J Mass Spectrom 198 (2000) 97–111) © 2000 Elsevier Science B.V.

Keywords: Mass spectrometer; Mass filter; Ion trap; Pulse signal

1. Introduction

The advent of a new rf signal waveform for quadrupole mass spectrometers calls for both better understanding of how the new signal transforms the stability diagram of QMS and careful examination of properties of ion trajectories within the rf field. In this article we show how the sensitivity of mass spectrometers can be increased and describe some of the difficulties that a developer using EC signals could face.

In the first part of this article (Sec. 2) we discuss the features of stability diagram configuration in the case of pulse and harmonic EC signals. We discovered that the adjacent stability zones overlap for certain pulse EC signals. Unexpectedly, an unstable zone appeared as a result of two adjacent stable zones overlapping.

In Sec. 3 we discuss in detail the amplitude-phase characteristics (APC) of ion movement within the rf fields. The distinguishing feature of these characteristics for EC signals is the presence of an extensive phase plateau (up to 0.5 of the period duration), where the amplitude of ion oscillation with initial zero velocity is close to the value of the initial coordinate. This plateau results in high sensitivity produced by EC signals. However, the plateau only appears under certain conditions, which are the subject of Sec. 3.

In the last section we present some experimental results for the ion trap driven by a pulse EC signal and a conventional pulse signal of rectangular waveform (meander).

* Corresponding author. E-mail: sheretov@eac.ryazan.su

1387-3806/00/$20.00 © 2000 Elsevier Science B.V. All rights reserved
PII S1387-3806(00)00164-0

We show that the experimental results completely match the theory. Use of the pulse EC signal substantially improves analysis parameters: sensitivity and quality factor (the product of sensitivity and mass resolution) are increased. At the same time, mass peak shape for the ion trap is dramatically improved (the developed theory does not predict this) [1,2]. Finally, we describe the experiment, which supports our assumption that the increase in sensitivity provided by the EC signal allows for easy implementation of QMS operation modes in high stability zones.

2. Stability diagram for EC signals

In Part I we showed that the harmonic EC signal can be written in the general form:

$$\psi(t) = a - 2q[\cos 2t + k \cos 2jt]$$

where a and q are conventional coefficients of the Mathieu equation. The value of the k coefficient is selected in accordance with the general property of the EC signal: the value of the $\psi(t)$ function in the optimal phase of the first kind must be equal to zero (for $a = 0$ and $k = 1$). $j = 2$ and $j = 3$ correspond to the two types of harmonic EC signal: asymmetric harmonic EC signal ($j = 2$), and symmetric harmonic EC signal ($j = 3$).

It can be seen from Fig. 1(a) and (b) that the configuration of general stability zones for the harmonic EC signal is similar to the configuration of corresponding zones for a conventional harmonic signal (Mathieu equation). However, depending on the value of j the general zones change their position. The largest change occurs when $j = 2$ (asymmetric signal). The upper zones become significantly offset. Table 1 illustrates this situation. It contains apex coordinates of the upper stability zones for the harmonic EC signals with $j = 2$ and $j = 3$ and for a conventional harmonic signal. The apexes are numbered clockwise starting with the apex closest to the stability diagram origin.

Because we have shown in Part I of this article $k = 1 + a/2q$, the following procedure may be used to select a mode of operation. First, the slope of the scan line $\lambda = a/q$ is selected. Then, using the selected λ, we calculate the value of $k = 1 + \lambda/2$, which defines the required ratio between the higher harmonic amplitude and the fundamental harmonic amplitude. During a mass spectrum scan the ratio $\lambda = U_{=}/2U_{\sim}$ must remain constant (where $U_{=}$ is the dc component and $U_{\sim}$ is the amplitude of the harmonic with maximal period). It appears that the easiest implementation of this operation mode would use mass scanning performed by varying the frequency in which the required working frequencies are generated by dividing the basic frequency two or three times whereas the rf voltage amplitude and the dc potential are kept constant. Using the mass scanning by varying the

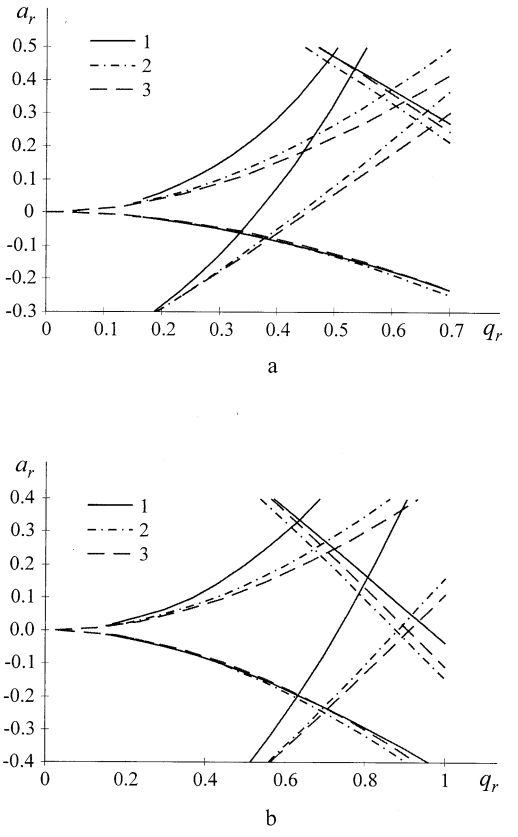

Fig. 1. The general stability zones for harmonic signal and harmonic EC signal. Line 1 is the general stability zone for the harmonic EC signal: $j = 2$; line 2 is the general stability zone for the harmonic EC signal: $j = 3$; line 3 is the general stability zone for the harmonic signal. (a) Axially symmetric ion trap; (b) the quadrupole mass filter.

Table 1
Coordinates of apexes for upper stability zones

Zone	Apex number	Harmonic EC signal, $j = 2$		Harmonic EC signal, $j = 3$		Harmonic signal	
		a	q	a	q	a	q
1-2	1	−1.8123785	2.5299805	−0.8630184	1.4016040	−1.2262803	1.7589171
	2	−1.9258433	2.6400262	−1.0041146	1.5344445	−1.4189715	1.9218195
	3	−1.7882954	2.6250547	−0.7517066	1.4878918	−1.2022845	1.8590730
	4	−1.8881137	2.7146157	−0.8809207	1.5892474	−1.3787012	1.9910923
2-1	1	1.1491935	0.7115880	1.6313973	1.3703163	2.4368040	2.1974819
	2	1.1482186	0.7267865	1.6305375	1.3897639	2.4383559	2.2036334
	3	1.9731550	0.8865319	2.3392184	1.6864042	3.3675018	2.7995565
	4	1.9696146	0.8910523	2.3317184	1.6941404	3.3667964	2.8011661

amplitude of the rf voltage has some practical difficulties because, in addition to the necessity in a constant λ, the ratio between amplitudes of the first and a higher harmonic must be kept constant.

More favorable is the mode of operation without a dc potential—the mass selective instability mode [3]. In this mode $k = 1$ and the amplitude of the basic and higher harmonics must be equal, which is relatively easy to implement, especially when the scanning is done by a changing frequency. The pulse EC signal [see Part I, Fig. 4(a) and (b)] creates wide capabilities for modification of the stability diagram. We will limit ourselves to consideration of the asymmetric EC signal as a simpler but nonetheless powerful tool for stability diagram transformation. Let us assume that the focusing pulse amplitudes and their duration [see Part I, positive pulses in Fig. 4(a)] are equal, and all η_i are multiples of $1/N$, where N is an integer. The first two conditions symmetrize the signal, and the third one simplifies its generation.

For the pulse EC signal we can use parameters a_1 and a_2, expressions that were introduced in Eq. (22-I) [i.e. Eq. (22) in Part I]. The use of these parameters allows us to draw stability diagrams for both the EC signal and a conventional pulse signal in the same system of coordinates [4].

In order to define a configuration of the general stability zones for the pulse EC signal we should find the appropriate function $\psi_i(t'_0)_{EC}$ [see Eq. (22-I)]. Determining the $\psi_i(t'_0)_{EC}$ functions is not difficult, but their expressions are bulky. However, the assumption that we have made above simplifies expressions for these functions:

$$\psi_1(t'_0)_{EC} = \psi_1(t'_0)_u|_{t'_0=0}$$

$$\psi_2(t'_0)_{EC} = \beta_u + \frac{1}{2}\eta_a(1 - 2t'_0)\psi_1(t'_0)_u|_{t'_0=0}$$

$$\psi_3(t'_0)_{EC} = \beta_u + \frac{1}{2}\eta_a(1 + 2t'_0)\psi_1(t'_0)_u|_{t'_0=0}$$

$$\psi_4(t'_0)_{EC} = \psi_4(t'_0)_u|_{t'_0=0} + \eta_a\beta_u + \frac{\eta_a^2}{4} \times [1 - 4(t'_0)^2]\psi_1(t'_0)_u|_{t'_0=0}$$

$$\psi_3(t'_0)_{EC} - \psi_2(t'_0)_u = 2\eta_a\psi_1(t'_0)_u|_{t'_0=0}$$

$$\beta_u = \frac{1}{2}[\psi_3(t'_0)_u + \psi_2(t'_0)_u] \quad (1)$$

where the values of the $\psi_i(t'_0)_{EC}$ functions are determined through the $\psi_i(t'_0)_u$ functions [Eq. (22-I)]; η_a is the relative duration of the active part of the EC signal; $\eta_1 = 2\eta_{1EC}$, and $\eta_2 = \eta_{2EC}$.

The $\psi_i(t'_0)_{EC}$ functions in Eq. (1) are determined for the initial phase of t'_0 within the active part η_a. The expressions for the other parts of the EC signal (η_{1EC} and η_{2EC}) can be similarly obtained.

The borders of the stability diagram for the pulse EC signal are described by the following equations:

$$\beta_{EC} = \frac{1}{2}[\psi_2(t'_0)_{EC} + \psi_3(t'_0)_{EC}] = \pm 1 \quad (2)$$

We see that β_{EC} does not depend on t'_0. Note that the function $\psi_1(t'_0)_u|_{t'_0=0}$ in Eq. (1) does not depend on t'_0 or on η_a. This allows us to find new expressions for

the stability zone boundaries. Let us write the fundamental equation

$$\psi_2(t'_0)_{EC}\psi_3(t'_0)_{EC} - \psi_1(t'_0)_{EC}\psi_4(t'_0)_{EC} = 1 \quad (3)$$

If all functions $\psi_i(t'_0)_{EC}$ in Eq. (3) are determined for a characteristic point lying on the respective stability boundary, then [as follows from Eqs. (1) and (2)] we have

$$\psi_2(t'_0)_{EC}|_{t'_0=0} = \psi_3(t'_0)_{EC}|_{t'_0=0} = \pm 1$$

In this case the following equation is valid on the stability zone boundaries:

$$\psi_1(t'_0)_{EC}|_{t'_0=0} \times \psi_4(t'_0)_{EC}|_{t'_0=0} = 0 \quad (4)$$

and for boundaries of the stability zones we have

$$\psi_1(t'_0)_{EC}|_{t'_0=0} = 0 \quad (5)$$

and

$$\psi_4(t'_0)_{EC}|_{t'_0=0} = 0$$

The obtained Eqs. (5) are equivalent to Eq. (2). Let us call stability zone boundaries that correspond to the first condition in Eq. (5) the ψ_1 boundaries, and those boundaries that correspond to the second condition will be called the ψ_4 boundaries (these terms are applicable for the respective zones).

The first zone on the stability diagram is the ψ_1 zone (we move from the origin along the a_1 axis). The second zone is the ψ_4 zone. The third zone is the ψ_1 zone again, i.e. zones ψ_1 and ψ_4 are interchanged on the stability diagram. The properties of upper stability zones are also changed from one zone to another.

The analysis of stability zone boundaries for the EC signal has shown that the ψ_1 zones may overlap with the ψ_4 zones when the value of η_a increases. For example, if η_a increases, then the second zone (the ψ_4 zone) descends on the stability diagram, and (under certain circumstances) overlaps with the ψ_1 zone. The overlapping of these zones starts from a point lying on the a_1 axis ($a_2 = 0$). The system of Eq. (5) can be solved if $\eta_2 = \eta_a$. There is no overlapping of zones when $\eta_2 > \eta_a$. If $\eta_2 < \eta_a$, then the intersection point of the ψ_1 boundary with the ψ_4 boundary moves from the a_1 axis into the stability diagram. In order to define the coordinates of the intersection point for ψ_1 and ψ_2 boundaries on the a_1 axis the following expression can be used:

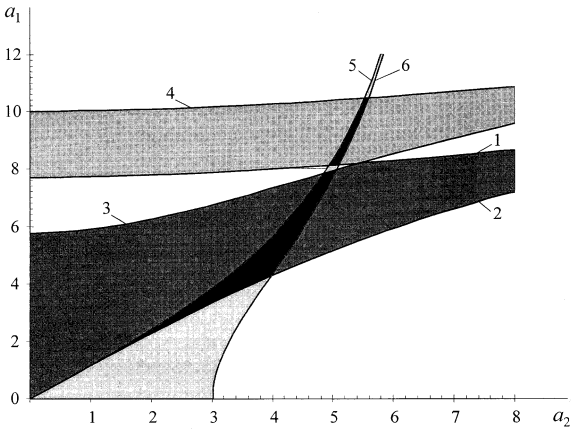

Fig. 2. The overlapped stability diagram for the axially symmetric ion trap in the case when the pulse EC signal (asymmetrical: $\eta_1 = 1/10$; $\eta_2 = 4/15$; $\eta_a = 8/15$) is applied to the electrodes. Lines 1 and 2 are the ψ_1 boundaries for the r coordinate, lines 3 and 4 are the ψ_4 boundaries for the r coordinate, and lines 5 and 6 are the ψ_1 boundaries for the z coordinate.

$$2\frac{\eta_1}{\eta_2} = a_1\eta_1 \tan \alpha_1\eta_1 \quad (6)$$

As mentioned above, the overlapped ψ_1–ψ_4 zones appear when $\eta_a > \eta_2$. The overlapped ψ_1–ψ_4 zones are unstable, whereas the nonoverlapping ψ_1 and ψ_4 zones are stable. The overlapping effect can be observed in Fig. 2. If a mass spectrometer operates in the upper apex of the first stability zone, this effect significantly deteriorates the performance. In this case the absolute value of stability parameter β in these nascent unstable zones is close to 1 near the borders, and changes very slowly with variation of the parameters a_1 and a_2. At the same time, sorting efficiency within the "unstable" zone is also decreased. Thus, when a mass spectrometer is driven by the pulse EC signal, stability zones can be divided into "regular" and "irregular" zones. The former zones correspond to $\eta_a < \eta_2$, and the latter zones correspond to $\eta_a > \eta_2$. The "regular" zones have the same structure for pulse EC signals, conventional pulse, and sinewave rf

signals. The "irregular" zones are distinguished by a pairwise merging of adjacent zones. The boundaries of these paired zones converge to one point (see Fig. 2). This corresponds to System (1) from which we can see that $\psi_4(t'_0)_{EC}$ substantially depends on η_a, whereas $\psi_1(t'_0)_{EC}$ does not. Therefore, the ψ_1 zones remain stationary with an increase in η_a, and the ψ_4 zones overlap the ψ_1 zones.

3. Amplitude-phase characteristics

As mentioned above, the shape of the $\delta_i(t_0)$ functions has a significant influence on the sensitivity of the QMS. These functions are inverse to the amplitude-phase characteristics of the first kind, and they were described by integrals (26-I) and (27-I) [integrals (26) and (27) in Part I].

We have compared shapes of the $\delta_i(t_0)$ functions for different EC signals. First, we have drawn stability zones for each signal applied to the axially symmetric ion trap. Then we chose the points close to apexes that correspond to the resolution close to 100. The resolution was determined using the points of intersection of the scan line, which passes through the chosen points, with the stability zone boundaries.

In Fig. 3 we compare the $\delta_i(t_0)$ functions calculated for the first stability zone 1-1 and for the upper zone 1-2 (Fig. 1) in the cases of a conventional harmonic signal, harmonic EC signal with $j = 2$, and $j = 3$. It can be seen from Fig. 3 that harmonic EC signals dramatically improve the shape of the $\delta_i(t_0)$ functions.

The values of integral (27) introduced in Part I are given in Table 2 for nine points lying close to apexes of stability zones (a resolution of about 100). We see that the maximal value of integral (27-I) for the first zone can be obtained by using harmonic EC signal with $j = 2$. This value is 7 times greater than the respective value of the integral for harmonic signals. An even better result was achieved for the second stability zone (zone 1-2). This zone is formed by the first zone for the r coordinate and the second zone for the z coordinate. The value of integral (27-I) here is 14 times greater! These calculations demonstrate that EC signals open the opportunities for wide use of the second zone in QMS operation. The smaller value of the integral (4 times smaller than in the first zone) is completely compensated for by a decrease in sorting time and improved peak shape.

However, functions (32-I) and (37-I) defined for the r coordinate within the second zone do not satisfy EC signal conditions. In this case the phase that corresponds to $\psi(t_0) = 0$ does not coincide with the optimal phase of the first kind. Our calculations show that there is no increase in the value of integral (27-I). We will return to this problem in the section devoted to the pulse EC signal.

We have noted above that harmonic EC signal in the mode with $a = 0$ has certain potential. This is due to the fact that amplitudes of the first, second, and third harmonics are equal to each other. The values of q_{border} that represent the intersection point of the z border with the $a = 0$ axis are given in Table 3.

Our calculations of integral (27-I) in a range of q from 0 to q_{border} have shown that the harmonic EC signal has advantages over the conventional harmonic signal. However, these advantages are not as strong in the case when an ion working point is located close to the upper apex of the stability zone (the use of the harmonic EC signal with $j = 2$ has the maximal advantage in the whole range). The value of the integral is about 1.1 for $q/q_{border} = 0.1$, and about 1.7 for $q/q_{border} = 0.9$.

We would like to draw the reader's attention to an important feature of the harmonic EC signal: the trapping efficiency is constant throughout the whole range of q (from 0 up to q_{border}). Integral (27-I) for the EC signal with $j = 2$ changes only by 16% within the range from $0.1q_{border}$ to q_{border}, whereas the change for the harmonic signal is 44%. This advantage plays an important role for substance identification.

We should note, however, that all estimations shown here are valid when the ion trap operates in the mass selective instability mode with radial electron beam injection.

If the ionization within the ion trap is done by using a sharp electron beam injected along the longitudinal axis (widely used at the present time), then the harmonic EC signal should be transformed in order to

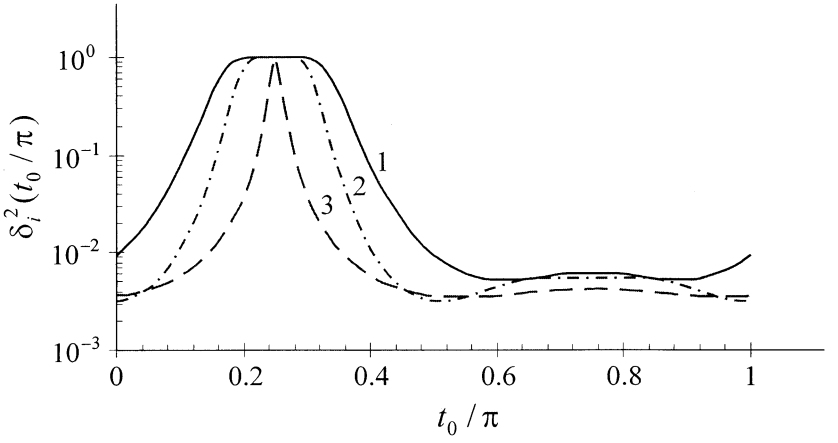

a

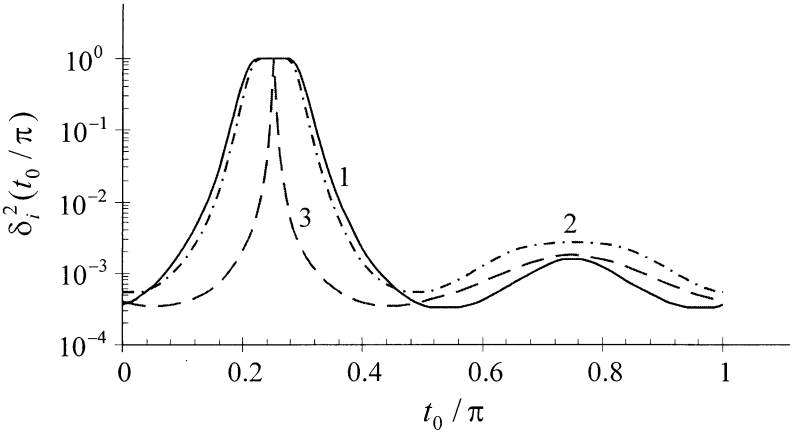

b

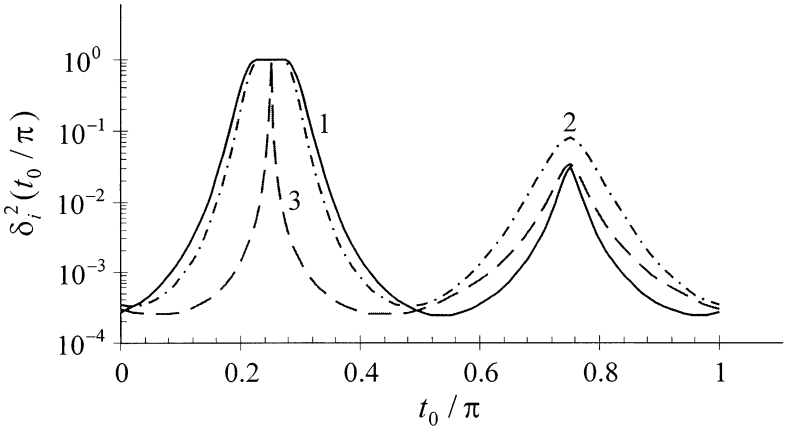

c

Fig. 3. The dependency between the $\delta_i^2(t_0)$ function and the initial phase t_0 for rf signals. Line 1 is the harmonic EC signal: $j = 2$. Line 2 is the harmonic EC signal: $j = 3$. Line 3 is the harmonic signal. (a) The upper apex of the first general zone; (b) the upper apex of the 1-2 zone; (c) the lower apex of the 1-2 zone.

Table 2
The values of integral (27-I) for points lying near apexes (a resolution of about 100)

Zone	Apex	Harmonic EC signal, $j = 2$	Harmonic EC signal, $j = 3$	Harmonic signal
1-1	Upper	0.090751	0.04389	0.012596
1-2	Upper	0.02357	0.020834	0.0017
	Lower	0.023532	0.024724	0.002397

satisfy condition (31-I) for the z coordinate. In this case the harmonic EC signal with $j = 2$ yields about a 7% gain in the value of the integral (27-I) for $q/q_{\text{border}} = 0.1$, and a 53% gain for $q/q_{\text{border}} = 0.9$. The gain increases when q approaches q_{border}.

As we have shown in Part I, the pulse EC signal most fully satisfies conditions (31-I). Before discussing the advantages of this signal, we should determine the conditions under which (31-I) are satisfied completely.

The pulse EC signal (Fig. 4, Part I) meets the first condition (31-I) within the active part η_a. Thus, in order to satisfy all conditions (31-I) there should be at least one root t_{0m} of equation $F_3(t'_0) = 0$ for η_a, and this root must provide the maximal value of $F_2(t_{0m})$. This implies that the active part of the EC signal incorporates the optimal phase of the first kind.

The phase t'_0 in Eq. (1) lies in the active part η_a. Considering Eq. (21-I), we can assert that function $F_3(t'_0)$ has only one root $t_{0m} = 0$ in the middle of η_a. In order for $F_2(t'_0)$ to have a maximum when $t_{0m} = 0$, the value of $\psi_1(t'_0 = 0)_u$ must be positive.

Thus, the condition

$$\psi_1(t'_0)_{\text{EC}}\big|_{t'_0=0} = 0 \tag{7}$$

describes a line on the stability diagram. This line divides the stability diagram into two parts: a part where conditions (31-I) can be satisfied and one where they cannot. Note, however, that Eq. (7) corresponds to the boundaries of ψ_1 zones [see Eq. (1)]. Evidently, within the ψ_1 zones and when $t_{0m} = 0$ the value of $F_2(t_{0m})$ is maximal, and the optimal phase of the first kind occurs during the active part η_a. This condition is satisfied for the ψ_4 zones. Amplitude-phase characteristics of the first kind in Fig. 4 are for characteristic points located within ψ_1 and ψ_4 zones of the stability diagram. The APC is typical for the pulse EC signal within the ψ_1 zones (oscillation amplitude is constant and equal to 1 during the active part η_a). For points lying in the ψ_4 zones oscillation amplitude greatly exceeds 1, and there are two optimal phases of the first kind out of η_a. The $Y_m(t_0)$ function rapidly varies around these phases.

Table 3
The values of q_{border} (the point of intersection of the z border with the $a = 0$ axis)

Harmonic signal	Harmonic EC signal, $j = 2$	Harmonic EC signal, $j = 3$
0.4540232	0.3661056	0.4395546

The shape of $\delta_i^2(t_0)$ functions is demonstrated in Fig. 5 for a conventional pulse signal (meander) and for pulse EC signals with different N. Working points were chosen near the apexes of the stability zones in order to set a resolution of about 100. Fig. 5 shows that $\delta_i^2(t_0)$ for the meander is a rapidly damped function around the optimal phase of the first kind, whereas the value of $\delta_i^2(t_0)$ for pulse EC signals is constant and equal to 1 within the active part η_a.

In Table 4 we compare the values of integral (27-I) for EC signals and meander. The data were obtained for points lying near the apexes of the stability zones with a resolution of about 100. It follows from Table 4 that for operation in the first stability zone the pulse EC signal yields 10 times the trapping efficiency of the meander in the radial plane. The trapping efficiency is 30 times greater (as in the case of the harmonic EC signal, see Table 2) when the ion trap operates in the second zone 1-2.

Another important feature of the pulse EC signal is that the trapping efficiency for ions in the first and second zones differs slightly. As shown above, this

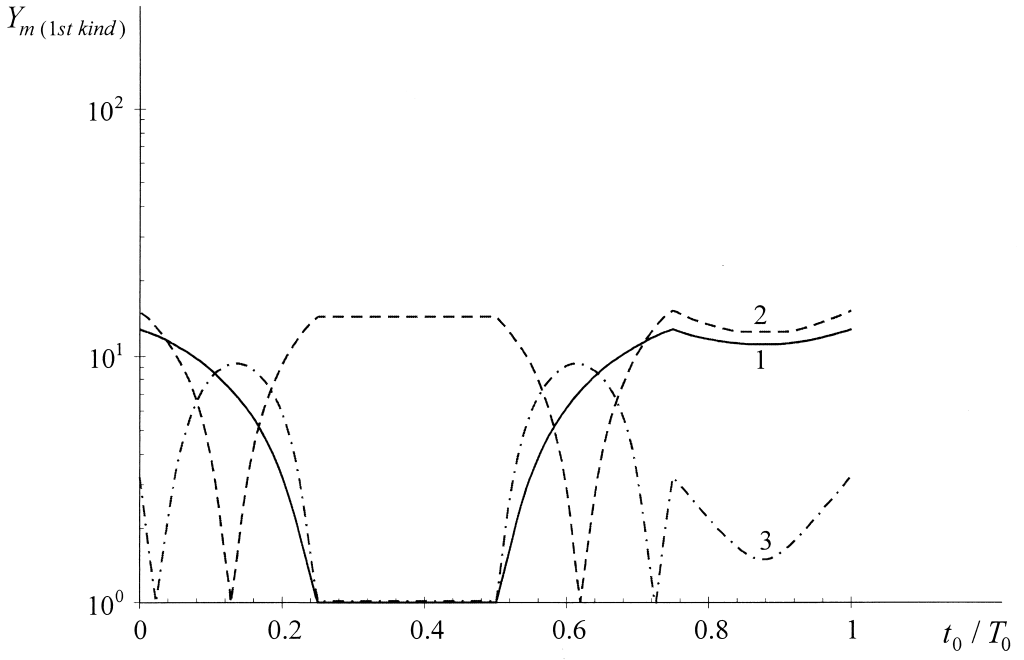

Fig. 4. Amplitude-phase characteristic of the first kind along the r coordinate for the ion trap; characteristic points of ions lie within ψ_1 and ψ_4 zones of the general stability diagram (pulse EC signal with $\eta_1 = \eta_2 = \eta_a = 1/4$). Line 1 is the upper apex of the first general zone (the r coordinate, the ψ_1 zone, a resolution of about 100; $a_1 = 4.403647$, $a_2 = 4.280470$, $\beta_u = -0.9946735$). Line 2 is the upper apex of the second zone 2-1 (the r coordinate, the ψ_4 zone, a resolution of about 100; $a_1 = 4.808551$, $a_2 = 11.091746$, $\beta_u = -0.9318303$). Line 3 is the middle of the third zone 3-1 (the r coordinate, the ψ_1 zone, a resolution of about 26000; $a_1 = 14.014088$, $a_2 = 6.446663$, $\beta_u = 0.4083183$).

enables a QMS to operate in upper stability zones. Comparing Tables 2 and 4 we note that pulse EC signals achieve 100–200 times the trapping efficiency of a conventional harmonic signal when the ion trap operates in apexes of the second stability zone.

4. Experimental

Experimental studies of theoretically predicted advantages of EC signals were conducted on the quadrupole mass filter and ion trap with a thin-walled axially symmetric electrode system that was developed in our laboratory for the VEGA space program (Venus and Haley's Comet exploration program) [5,6]. Experiments on the ion trap were done using the pulse EC signal that was formed by applying the unipolar rf pulses to the ring and endcap electrodes, as shown in Fig. 6. The amplitude of pulse rf voltage applied to the ring electrode was varied within 235–245 V. The pulse rf voltage with an amplitude of 220 V was applied to the endcap electrodes. The mass scanning was performed by synchronously varying a frequency of both rf signals.

The experiment involved a comparative analysis of various factors and their influence on the peak shape of *m/z* 28. A conventional pulse signal (meander) was formed by applying one unipolar pulse signal to the endcap electrodes and a dc potential to the ring electrode. It was possible to compare parameters of mass peaks obtained by application of various rf signals to electrodes of the analyzer. The use of the same electrode system, one pulse generator, and one control system ensures the correct comparison of the obtained experimental results. In the experiments we used a conventional clean pumping system, and a channel multiplier as a detector of ions. Operational

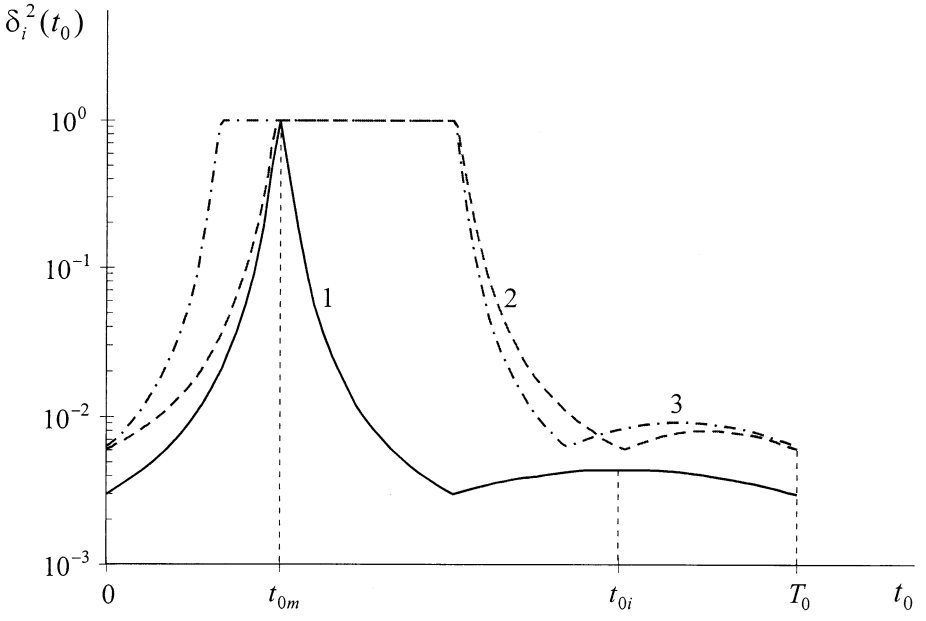

Fig. 5. The dependency between the $\delta_i^2(t_0)$ function and the phase t_0 for various signals: Line 1 is the pulse signal meander ($a_1 = 3.584338$, $a_2 = 2.505884$, $\beta_u = 0.977079$). Line 2 is the pulse EC signal with $N = 4$ ($\eta_1 = \eta_2 = \eta_a = 1/4$; $a_1 = 4.403648$, $a_2 = 4.28047$, $\beta_u = 0.938231$). Line 3 is the pulse EC signal with $N = 6$ ($\eta_1 = 1/6$; $\eta_2 = \eta_a = 1/3$; $a_1 = 5.376507$, $a_2 = 3.758827$, $\beta_u = 0.949264$).

mode and data acquisition were computer controlled. Relative sensitivity I_0, maximal resolution, peak shapes, and quality factor Q were chosen as criteria for comparison of operation modes. The quality factor is the product of relative sensitivity I_0 and resolution defined at a certain level of a peak height.

Experimental studies of the quadrupole mass filter were done on the electrode system developed in our laboratory for the Mars 96 space program. The electrode system is 200 mm long, and the field radius is 8.2 mm. We have also developed an original pulse generator forming an antipodal pulse EC signal. The mass scanning was performed by varying the frequency of the rf signal. The frequency tuning range is (0.01–1) $\times$ 10^6 Hz; the short term frequency instability is better than 3×10^{-5}; the pulse front time is less than 30×10^{-9} s.

A dynamic mass spectrometer with a stable particle confinement yields a mass peak with three parts. The first part of the peak corresponds to the stable (bounded) ion trajectories. Two other parts correspond to the unstable trajectories, features of which determine the mass peak tails. However, sensitivity of an instrument depends on the movement of ions whose working points lie within a stable region of the stability diagram. Thus, the purpose of the experimen-

Table 4
The values of integral (27-I) for pulse EC signals and meander

Zone	Apex	Pulse EC signal			Meander
		$N = 4$	$N = 6$	$N = 8$	
1-1	Upper	0.3	0.37	0.4	0.039
1-2	Upper	0.26	0.344	0.383	0.017
	Lower	0.264	0.345	0.385	0.019

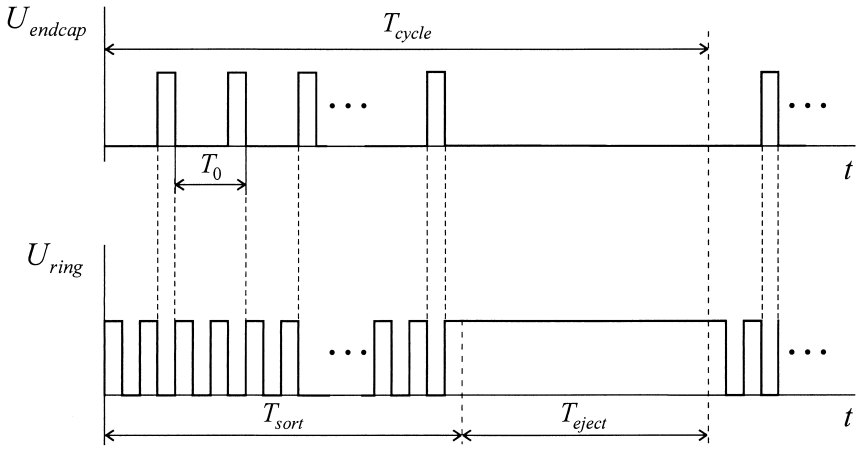

Fig. 6. Unipolar rf pulse voltages applied to electrodes of a three-dimensional axially symmetric ion trap. The scan function forms pulse EC signals. U_{endcap} is the potential of the endcap electrodes; U_{ring} is the potential of the ring electrode; T_{sort} is the sorting time; T_{eject} is the ejection time for sorted ions; T_{cycle} is the duty cycle.

tal treatment of the pulse EC signal is to compare the sensitivities obtained with the pulse EC signal and a conventional pulse signal—meander. We have previously shown in [1] that the pulse EC signal yields an enhanced peak shape in comparison with "meander." We have compared peaks with a relative intensity of 1. Mass peaks of *m/z* 28 Da obtained with a three-dimensional ion trap operating in the mode of mass-selective storage and driven by the pulse EC signal and "meander" are shown in Fig. 7. We can see that in addition to a better peak shape, the pulse EC signal yields sensitivity at least 100 times better than that obtained with meander.

Fig. 8 shows the relative sensitivity of the ion trap measured at *m/z* 28 as a function of mass resolution for the pulse EC signal and meander. We see that

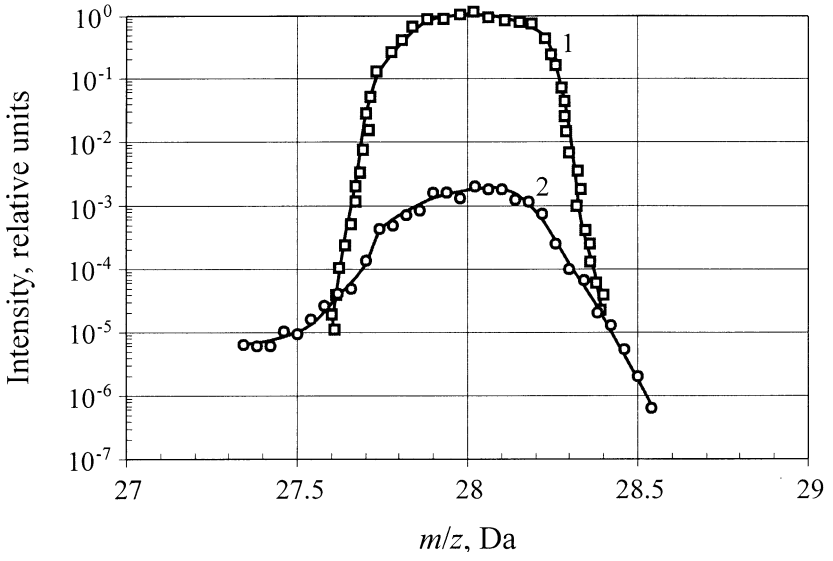

Fig. 7. Mass peaks of *m/z* 28 Da obtained with a three-dimensional ion trap operated in the upper apex of the first stability zone in the mass-selective storage mode. Line 1 is the asymmetrical pulse EC signal with $\eta_1 = \eta_a = \eta_2 = 1/4$; line 2 is the meander.

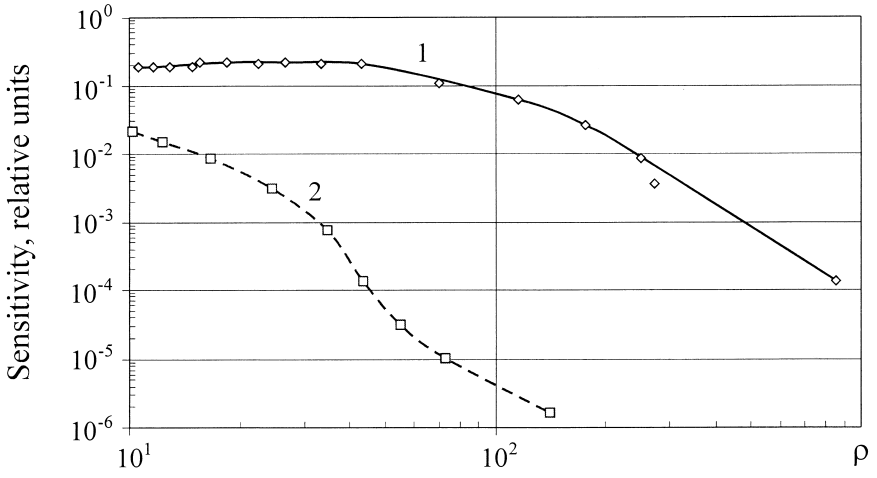

Fig. 8. Experimental variation of the relative sensitivity (*m/z* 28) as a function of a resolution ρ defined at level 0.1 from the peak height. Line 1 is the pulse EC signal ($\eta_1 = \eta_2 = \eta_a = 1/4$); line 2 is the meander.

sensitivity in the case of the pulse EC signal is 10 times greater than the sensitivity of meander for low resolutions. Sensitivity increases with resolution (see Fig. 8), and for a resolution of about 100 we obtain several orders sensitivity of the meander. The maximal resolution for the pulse EC signal obtained in the experiments is above 1000, and a further comparison of sensitivities becomes moot. Comparison of the curves in Fig. 8 can yield another remarkable property of the pulse EC signal: sensitivity of the ion trap is constant up to a resolution of about 100 (sensitivity in the case of meander traditionally fades when resolution increases). This property is due to the fact that the ion oscillation amplitude is constant when a working point moves on the stability diagram up to stability zone boundaries for any phase within the active part of the EC signal. In the case of meander the oscillation amplitude increases when a working point approaches the boundaries for all phases within the focusing pulse along the *r* coordinate (an exception is one point—the optimal phase of the first kind).

Observed dependency between the quality factor and resolution is shown in Fig. 9 for both signals. Again, the quality factor for meander traditionally decreases when resolution increases, whereas the quality factor for the pulse EC signal increases when a resolution increases, and decreases for higher resolutions.

For higher resolutions and for a greater quality factor (by a factor of 100) we achieve 4–5 times the resolution of meander (resolution of about 1000 at 1% peak height). Thus, experiments with the pulse EC signal showed greater sensitivity than the sensitivity predicted from the model. From our point of view, this remarkable mismatch of theory and experiments follows from incorrect comparison of sensitivities for equal resolutions. We have demonstrated [2] that the pulse EC signal considerably shortens the mass peak tails caused by the unstable ions. Thus, the real resolution ρ for the pulse EC signal greatly exceeds the theoretical one that was defined using the points of intersection of the scan line with the stability zone boundaries.

We first became interested in the operation in upper zones in the early 1980's during the ion trap development for the VEGA space program (Venus and Haley's Comet exploration program). The results of experiments have been described in [7]. However, we could not find sufficient theoretical or experimental justification for operation in upper zones. Even the use of an electrode system with elliptical electrodes gives about 100 times smaller sensitivity than the sensitivity for operation in the upper apex of the first stability zone. Further attempts to operate in upper zones on the quadrupole mass filter utilizing a pulse signal were unsuccessful (an exception is the opera-

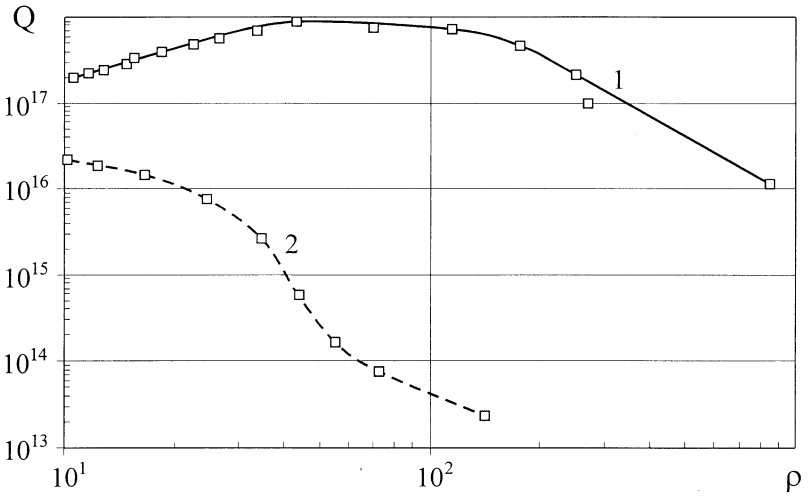

Fig. 9. Experimental variation of the quality factor Q as a function of a resolution ρ defined at level 0.1 from the peak height. Line 1 is the pulse EC signal ($\eta_1 = \eta_2 = \eta_a = 1/4$); line 2 is the meander.

tion in the middle of the second zones with a resolution of about 20). Thus, when the theory showed a radical solution to the problem with sensitivity in upper zones, we planned an experiment using the quadrupole mass filter developed and tested for the Mars 96 space program.

The general stability diagram for the mass filter operating with the pulse EC signal is shown in Fig. 10 ($\eta_1 = 1/6$; $\eta_a = \eta_2 = 1/3$). In this figure we also show scaled-up upper zones 1-2, 1-3, and the scan lines that pass through the middle of the respective zones and produce theoretical mass resolutions $\rho_{1\text{-}2} = 19$ and $\rho_{1\text{-}3} = 410$. In this case one-dimensional sorting along the y coordinate can be implemented (the pulses around η_a are focusing for this coordinate). If the slope of the scan line is changed from λ_0 (corresponding to the middle of a zone where $\beta_x = \beta_y = 0$), and the scan line approaches the upper or lower apex of the stability zone, the resolution increases and one-dimensional sorting transforms to the mode of operation in the apex of stability zone.

Experimental mass resolution for *m/z* 18, defined at 50% peak height, as a function of the scan line slope is demonstrated in Fig. 11 for operation in the 1-2 zone (a), and 1-3 zone (b). The respective variations of a theoretical resolution are also shown. Notice that the experimental resolution matches the theoretical one for zone 1-2.

A mass spectrum around *m/z* 18 Da is shown in Fig. 12. The maximal resolution obtained in the upper apex is greater than resolution for the lower apex. The same effect was observed for zone 1-3. Minimal experimental resolution for zone 1-2 coincides with a theoretical value ($\rho_0 = 19$, $\rho_{\text{exp}} = 20$). These values for zone 1-3 are different ($\rho_0 = 410$, $\rho_{\text{exp}} = 320$). The difference in resolution occurs because a sorting time in the 1-3 zone is two times less than in the 1-2 zone, which causes the minimal resolution decrease. In the experiments the minimal ion energy was set greater than or equal to 2 eV. This energy corresponds to a sorting time $n_{\text{sort}} = 18$ for the middle of the 1-2 zone, and $n_{\text{sort}} = 9$ for the middle of zone 1-3. Note that a transition region in the mass filter increases velocity spread in longitudinal directions and causes the real sorting time to decrease.

The obtained experimental data allow us to analyze the dependence of the quality factor on the scan line slope for zones 1-2 and 1-3. If the scan line is shifted from the lower apex of the 1-2 zone to the upper one, the quality factor increases by a factor of 10. A region of the maximal quality factor for zone 1-3 is located close to the lower apex, and a variation in the quality

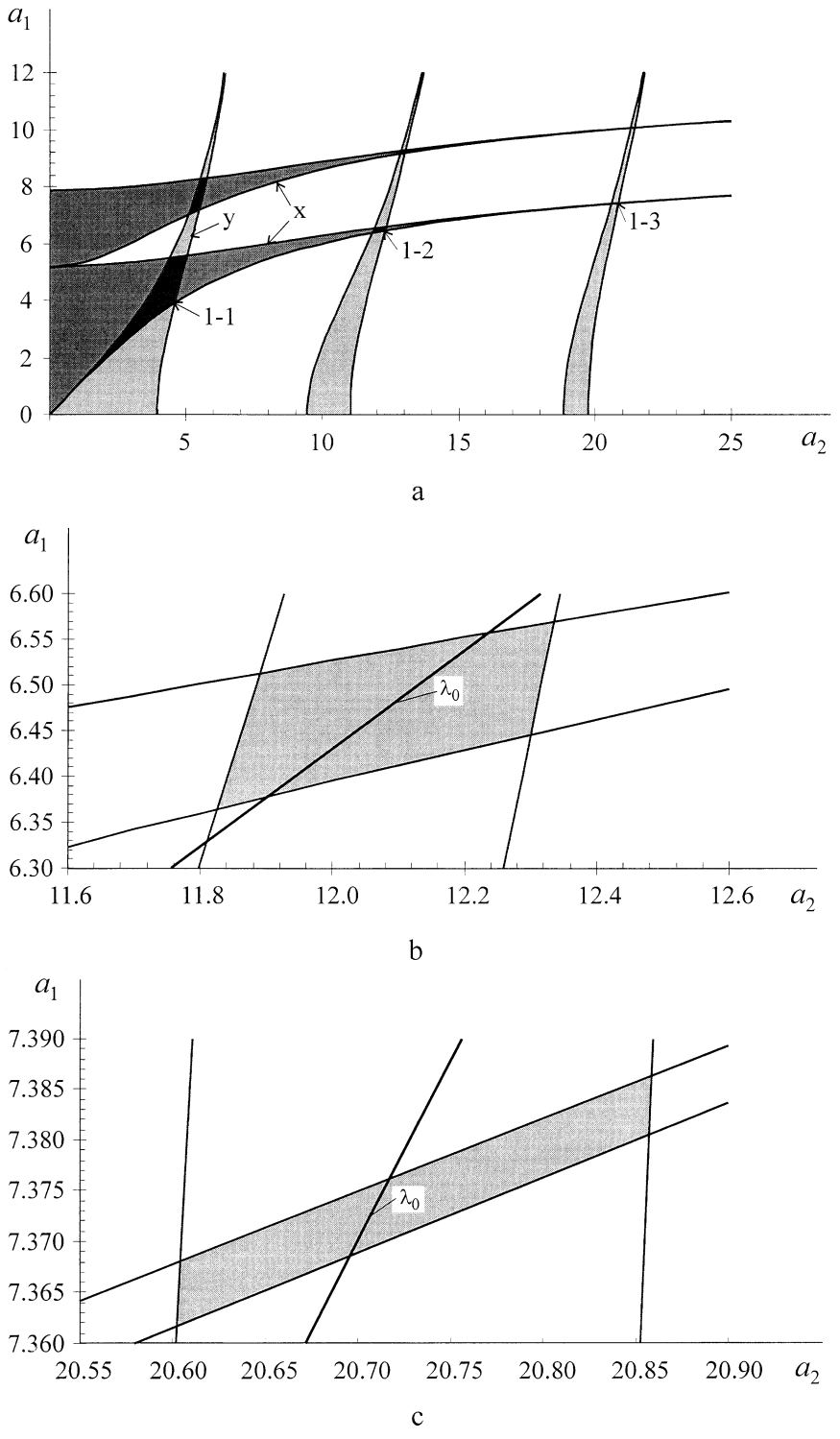

Fig. 10. Overlapped stability diagram for the quadrupole mass filter driven by pulse EC signal ($\eta_1 = 1/6$, $\eta_2 = \eta_a = 1/3$, $N = 6$). (a) The general stability diagram; (b) zone 1-2 and the scan line that passes through the middle of the zone; (c) zone 1-3 and the scan line that passes through the middle of the zone.

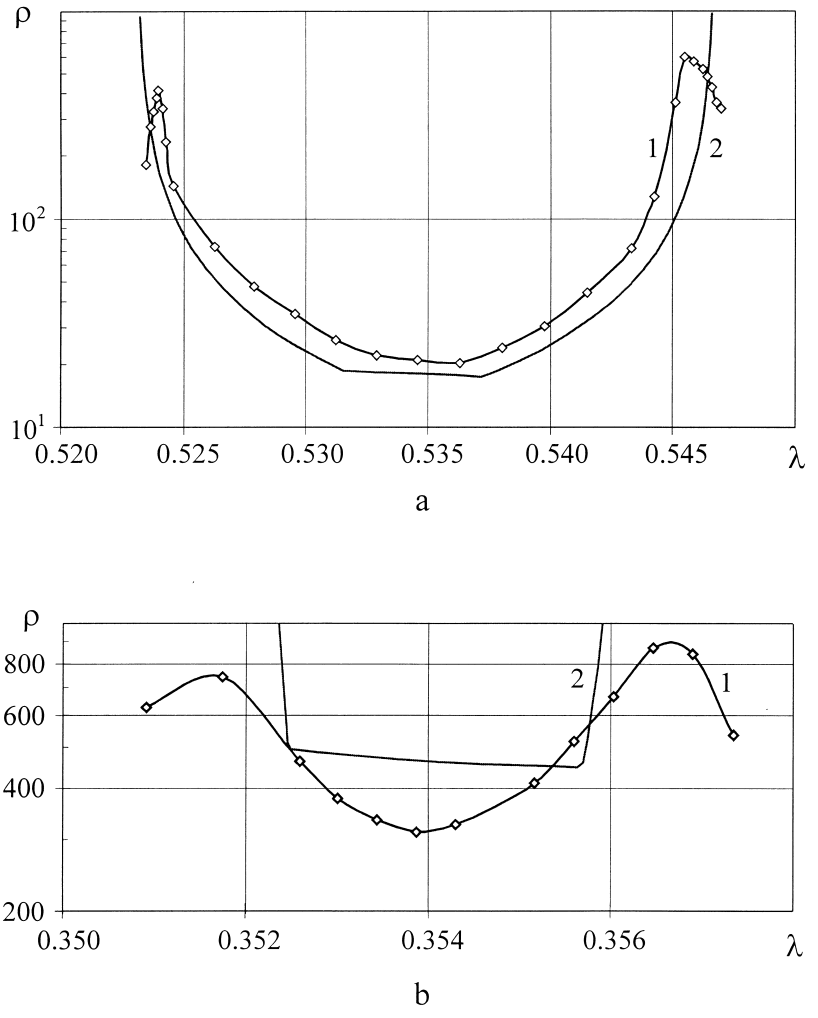

Fig. 11. Resolution (*m/z* 18) as a function of the scan line slope for operation with a pulse EC signal in upper zones. Line 1 is experiment; line 2 is theory. (a) Zone 1-2; (b) zone 1-3.

factor within this zone is the same. We should note, however, that the mean value of the quality factor is constant within both zones.

5. Conclusions

In this article we attempt to draw the attention of our colleagues to opportunities for possible improvements of QMS performance that lie in optimal transformation of the rf signal waveform. The experiment described in the article has been directed solely toward the validation of theoretical conclusions regarding the proposed EC signals. Only time will tell whether or not the next-generation QMS will employ EC signals; we can only hope that it will happen.

Acknowledgements

The authors thank Andrei E. Sheretov, who contributed the original software that enabled us to begin our findings. We are also grateful to E.W. Mamontov, who developed the original electronics module used

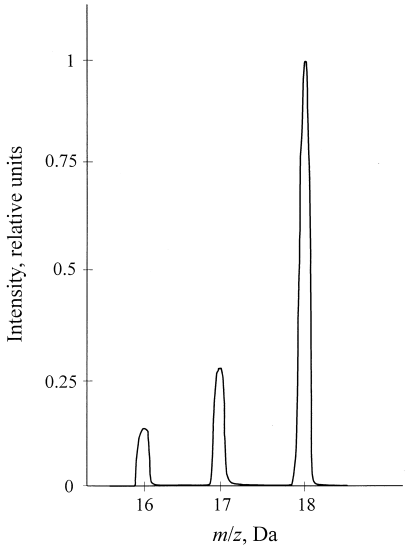

Fig. 12. A mass spectrum around *m/z* 18 Da obtained with the quadrupole mass filter operated in the upper apex of the 1-2 zone in the case of asymmetrical pulse EC signal ($\eta_1 = 1/6$; $\eta_a = \eta_2 = 1/3$).

in the experiments. We thank Igor W. Philippov for his assistance in preparing this manuscript, and acknowledge gratefully the work of referees whose valuable comments allowed us to obviate apparent mistakes.

References

[1] E.P. Sheretov, B.I. Kolotilin, A.E. Sheretov, Proceedings of the 14th International Mass Spectrometry Conference, Tampere, Finland, August 1997, p. 229.
[2] E.P. Sheretov, T.B. Karnav, A.V. Brykov, Int. J. Mass Spectrom. 190/191 (1999) 113.
[3] G.C. Stafford, P.E. Kelley, J.E.P. Syka, W.R. Reynolds, J.F.J. Todd, Int. J. Mass Spectrom. Ion Processes 60 (1984) 85.
[4] E.P. Sheretov, W.I. Terent'ev, J. Tech. Phys. 12 (1972) 953.
[5] Y.A. Surkov, F.F. Kirposov, O.P. Soborcev, V.N. Glasov, A.G. Dunchenko, L.P. Taciy, Astron. Lett. 12 (1986) 114.
[6] E.P. Sheretov, V.S. Gurov, M.P. Safonov, I.W. Philippov, Int. J. Mass Spectrom. 189 (1999) 9.
[7] E.P. Sheretov, M.P. Safonov, B.I. Kolotilin, S.P. Ovchinnikov, V.S. Gurov, N.V. Veselkin, A.P. Borisovstiy, W.I. Banin, J. Tech. Phys. Lett. 15 (1989) 85.